

Magic angle twisted bilayer graphene as a highly efficient quantum Otto engine

Ayush Singh* and Colin Benjamin†

School of Physical Sciences, National Institute of Science Education and Research, HBNI, Jatni 752050, India

At a discrete set of *magic angles*, twisted bilayer graphene has been shown to host extraordinarily flat bands, correlated insulating states, unconventional superconductivity, and distinct Landau level degeneracies. In this work, we design a highly efficient quantum Otto engine using a twisted bilayer graphene sample. Flat bands, which occur at magic angles, make the prospect of extracting useful work from our Otto engine lucrative. We use an eight-band continuum model of twisted bilayer graphene to compute efficiencies and work outputs for magic and non-magic angle twists, and compare the results with an *AB* stacked bilayer and a monolayer. It is observed that the efficiency varies smoothly with the twist angle and the maximum is attained at the magic angle.

I. INTRODUCTION

One of the ways to approach quantum thermodynamics is to design and study thermodynamic cycles designed as quantum analogues of classical thermodynamic processes. These cycles use quantum matter as “working substance” to convert thermal energy to useful work. In the literature, quantum analogues of adiabatic, isochoric, isothermal [1] and isobaric [2] process have been described, and some general results with quantum thermodynamic cycles, like Carnot and Otto, have been derived [1–4].

Due to quantum nature of working substance, quantum heat engines (QHEs) are expected to exhibit some special properties that allow better performance than their classical counterparts. For example, it has been shown that quantum heat engines can extract work from a single heat bath [5], and under certain conditions even surpass the Carnot limit [6, 7]. Hence, QHEs can be used to efficiently convert thermal energy to useful work in nanoscale devices. In addition to this, studying quantum thermodynamic cycles gives us an opportunity to test the robustness of thermodynamic principles in a quantum setting. Moreover, since the language used to describe QHEs is so general, the same discussion can be applied to phenomena ranging from lasers and photosynthetic light harvesting [7–9] to information theory and quantum computation [10, 11].

Quantum thermodynamic processes are carried out either by quasistatically changing the temperature of the heat reservoir—which the working substance is kept in equilibrium with—or by varying some tunable parameter that changes the energy spectrum of the quantum system. In magnetically driven quantum heat engines, Landau levels are changed by varying an external magnetic field [12, 13]. This is convenient because it is generally easier to quasistatically modulate the external field than some internal parameter of the working substance [12]. Magnetically driven quantum heat engines based on a semiconductor quantum dot [12, 13] and monolayer graphene flake [14, 15] have been proposed, however, these are by no means the only kinds of QHEs possible.

In this paper, we propose a magnetically driven quantum heat engine based on twisted bilayer graphene (TBG). At a discrete set of magic angles, TBG hosts exceptionally flat electronic

bands where Fermi velocity vanishes and the two layers get strongly coupled [16, 17]. Moreover, twisted bilayer graphene near the first magic angle shows some unusual behaviour for which there are no satisfactory theoretical explanations, such as correlated insulating states at half-filling [18], unconventional superconductivity [19], discernibly different butterfly spectra and a distinct sequence of Landau level degeneracies [20, 21]. All of this makes TBG a very exciting candidate as working substance in a quantum heat engine.

In this paper, we present calculations for a quantum analogue of the Otto cycle [1, 3, 22] with TBG as working substance and observe that the efficiency in *AB* stacked bilayer is better than what is observed for both monolayer graphene and semiconductor quantum dot, although the quantum dot approaches bilayer efficiency at large magnetic fields. Moreover, the efficiency further increases when twist is added and achieves a maximum at the magic angle. For computing Landau levels in TBG, we use an eight-band approximation of the non-interacting continuum model Hamiltonian [16, 17, 23, 24] which reproduces the Fermi velocity with reasonable accuracy down to the first magic angle [16], and diagonalize it numerically [25].

The rest of this paper is organized as follows: in the next section, we review Landau levels in monolayer and bilayer graphene, and then give a detailed procedure for calculating Landau levels in magic angle twisted bilayer graphene (MATBG). In Section III, we describe the quantum Otto engine cycle and derive expressions for both work output and efficiency. In Section IV, we present results for the work and efficiency in a tabular format, and compare results for the quantum Otto engines based on monolayer and bilayer graphene. Finally in Section V, we conclude with a perspective on future endeavours.

II. LANDAU LEVELS IN MONOLAYER AND BILAYER GRAPHENE

Since we propose a quantum heat engine which uses a graphene flake under transverse magnetic field as working substance, we start with a brief review of Landau levels in monolayer and bilayer graphene. The treatment here closely follows [26] for monolayer and [27] for bilayer graphene.

The effective low energy Hamiltonian for monolayer graphene near valley points is [26]

$$h_m(\mathbf{k}) = \xi \hbar v_F \boldsymbol{\sigma} \cdot \mathbf{k}, \quad (1)$$

* ayush.singh@niser.ac.in

† colin@niser.ac.in

where $\xi = \pm$ is the *valley pseudospin*, $v_F \sim 10^6 \text{ m s}^{-1}$ is Fermi velocity, $\sigma = (\sigma_x, \sigma_y)$ are Pauli matrices, and $\mathbf{k} = (k_x, k_y)$ is crystal momentum. This Hamiltonian leads to massless Dirac fermions with Berry phase π [26, 28]. In order to incorporate magnetic field we use the gauge transformation $\mathbf{p} \rightarrow \mathbf{p} + e\mathbf{A}$, where \mathbf{A} is magnetic vector potential and charge of electron is $-e$. For a transverse magnetic field $\mathbf{B} = (0, 0, B)$, vector potential in Landau gauge becomes $\mathbf{A} = (0, Bx, 0)$ which results in $\pi_x = p_x$ and $\pi_y = p_y + eBx$. With canonical commutation relations $[x_i, p_j] = i\hbar\delta_{ij}$, it can be shown that the operators,

$$\Pi = \frac{1}{\sqrt{2e\hbar B}}(\pi_x - i\pi_y) \quad \text{and} \quad \Pi^\dagger = \frac{1}{\sqrt{2e\hbar B}}(\pi_x + i\pi_y), \quad (2)$$

satisfy the algebra of harmonic oscillator ladder operators i.e., $[\Pi, \Pi^\dagger] = 1$. In terms of these ladder operators the Hamiltonian (1) can be written as,

$$h_m = \xi\sqrt{2}\frac{\hbar v_F}{l_B} \begin{bmatrix} 0 & \Pi \\ \Pi^\dagger & 0 \end{bmatrix}, \quad (3)$$

where we have introduced *Landau radius* $l_B = \sqrt{\hbar/eB}$. Eigenvalue equation for (3) can be solved exactly to give Landau levels for monolayer graphene [26],

$$E_n = \pm \frac{\hbar v_F}{l_B} \sqrt{2n}, \quad n = 1, 2, 3, \dots \quad (4)$$

where \pm is the *band index* labelling conduction and valence bands, and n is Landau level index. We neglect Zeeman splitting and note that each n -state is fourfold degenerate due to spin and valley degeneracies. For $n = 0$, we get a fourfold degenerate ground state at zero energy.

In tight-binding model for AB stacked bilayer graphene, there are four nearest-neighbour tunnelling processes: intralayer hopping, dimer hopping and two non-dimer hoppings, characterized by hopping energies $\gamma_0, \gamma_1, \gamma_3$ and γ_4 respectively, and we get massive Dirac fermions with Berry phase 2π [27, 29]. If we only consider intralayer and dimer hoppings in tight-binding model, a low energy Hamiltonian can be derived, which admits an analytical solution for Landau levels,

$$E_n = \pm \hbar\omega_B \sqrt{n(n-1)}, \quad n = 2, 3, 4, \dots \quad (5)$$

where $\omega_B = eB/m_{\text{eff}}$ is *cyclotron frequency* with effective mass $m_{\text{eff}} \approx 0.035m_e$ [27, 29]. Like in case of monolayer, each n state is fourfold degenerate due to spin and valley degeneracies, but both $n = 0$ and $n = 1$ are zero energy states and ground state is therefore eightfold degenerate. However, this spectrum is valid only for small level index and low magnetic fields because, in obtaining (5), the trigonal warping term was dropped and orbitals relating to dimer sites were eliminated [27]. In particular, we require $n\hbar\omega_B \ll 3 \text{ eV}$, which is easy to satisfy for a heat engine operating around 100 K in which only first few Landau levels are occupied.

A. Model for twisted bilayer graphene

The low energy continuum model Hamiltonian for twisted bilayer graphene consists of three parts: two single layer

Hamiltonians for intralayer hopping and a term for tunnelling between layers [16, 17, 23]. The single layer Hamiltonian, rotated by an angle θ for an isolated graphene sheet near Dirac point is

$$h_\theta(\mathbf{k}) = \mathcal{D}(\hat{z}, \theta) \left[-\hbar v_F \boldsymbol{\sigma} \cdot \mathbf{k} \right] \mathcal{D}^{-1}(\hat{z}, \theta), \quad (6)$$

where $\mathbf{k} = (k_x, k_y)$ is crystal momentum, $\boldsymbol{\sigma} = (\sigma_x, \sigma_y)$ are Pauli matrices and $\mathcal{D}(\hat{z}, \theta) = e^{-i\sigma_z\theta/2}$ is rotation matrix. Dirac points of the two rotated graphene layers are separated by $k_\theta = (8\pi/3a) \sin(\theta/2)$, where $a = 2.46 \text{ \AA}$ is lattice constant [16]. For interlayer tunnelling, an analysis of Moiré patterns shows that, for small twist angles there are three main tunnelling processes, with hopping directions (see Fig. 1)

$$\mathbf{q}_b = k_\theta(0, -1), \quad \mathbf{q}_{tr} = k_\theta\left(\frac{\sqrt{3}}{2}, \frac{1}{2}\right), \quad \mathbf{q}_{tl} = k_\theta\left(-\frac{\sqrt{3}}{2}, \frac{1}{2}\right),$$

which are characterized by matrices,

$$T_b = \begin{bmatrix} 1 & 1 \\ 1 & 1 \end{bmatrix}, \quad T_{tr} = \begin{bmatrix} e^{-i\phi} & 1 \\ e^{i\phi} & e^{-i\phi} \end{bmatrix}, \quad T_{tl} = \begin{bmatrix} e^{i\phi} & 1 \\ e^{-i\phi} & e^{i\phi} \end{bmatrix} \quad (7)$$

where $\phi = 2\pi/3$ [16, 24, 30]. Repeated hopping generates a honeycomb lattice in the momentum space. Truncating the continuum model Hamiltonian [16, 17, 23] at the first honeycomb shell, gives rise to the following eight-band Hamiltonian:

$$\mathcal{H}_\theta = \begin{bmatrix} h_{\theta/2}(\mathbf{k}) & wT_b & wT_{tr} & wT_{tl} \\ wT_b^\dagger & h_{-\theta/2}(\mathbf{k}_b) & 0 & 0 \\ wT_{tr}^\dagger & 0 & h_{-\theta/2}(\mathbf{k}_{tr}) & 0 \\ wT_{tl}^\dagger & 0 & 0 & h_{-\theta/2}(\mathbf{k}_{tl}) \end{bmatrix}, \quad (8)$$

where $\mathbf{k}_j = \mathbf{k} + \mathbf{q}_j$ and $w \approx 110 \text{ meV}$ is the interlayer hopping energy [16, 25]. The Hamiltonian \mathcal{H}_θ acts on a four-dimensional vector of two-component spinors, which is why it is called an eight-band model [25].

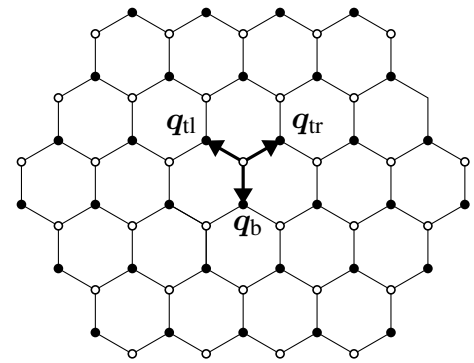


FIG. 1. Momentum space lattice of twisted bilayer graphene. Three equivalent Dirac points result in three distinct tunnelling processes. For all three processes $|\mathbf{q}_j| = k_\theta$ and the hopping directions are: $(0, -1)$ for \mathbf{q}_b , $(\sqrt{3}/2, 1/2)$ for \mathbf{q}_{tr} and $(-\sqrt{3}/2, 1/2)$ for \mathbf{q}_{tl} .

The angle dependence of h_θ is parametrically small and can be neglected, and it was shown in [16] that the eight-band approximation reproduces correct Fermi velocity with

reasonable accuracy to the first magic angle. Up to a scale factor, electronic structure of the eight-band model depends on dimensionless parameter $\alpha = w/\hbar v_F k_\theta$, in terms of which we can write renormalized Fermi velocity [16],

$$\frac{v'_F}{v_F} = \frac{1 - 3\alpha^2}{1 + 6\alpha^2}, \quad (9)$$

which vanishes at $\theta^* \approx 0.96^\circ$. This is where the magic angle occurs in the model. Moreover, it is the only magic angle the eight-band model can reproduce, since we are truncating the momentum space lattice at the first honeycomb shell. Refs [21, 24, 31] describe, in detail, the procedure for obtaining Landau levels in TBG, with full continuum model Hamiltonian.

Like in case of monolayer, we use the gauge transformation $\hbar\mathbf{k} = \mathbf{p} \rightarrow \pi = \mathbf{p} + e\mathbf{A}$ with $\mathbf{A} = (0, Bx, 0)$ to incorporate a transverse magnetic field and introduce ladder operators

$$\Pi = \frac{1}{\sqrt{2e\hbar B}}(\pi_x - i\pi_y), \quad \Pi^\dagger = \frac{1}{\sqrt{2e\hbar B}}(\pi_x + i\pi_y). \quad (10)$$

Since ladder operators obey $[\Pi, \Pi^\dagger] = 1$, we have harmonic oscillator states $|0\rangle, |1\rangle, |2\rangle, \dots$ satisfying $\Pi^\dagger \Pi |n\rangle = n |n\rangle$. These states constitute a complete, orthonormal basis set for this Hilbert space. Π^\dagger and Π act as raising and lowering operators for these states with $\Pi^\dagger |n\rangle = \sqrt{n+1} |n+1\rangle$ and $\Pi |n\rangle = \sqrt{n} |n-1\rangle$. Using these relations, it can be verified that the matrix representation of ladder operators in this basis is

$$\langle n | \Pi | m \rangle = \sqrt{m} \delta_{n,m-1} \quad \text{and} \quad \langle n | \Pi^\dagger | m \rangle = \sqrt{m+1} \delta_{n,m+1}. \quad (11)$$

To find Landau level spectrum, the substitution $\hbar\mathbf{k} \rightarrow \pi$ is made in (6) and the Hamiltonian is written in terms of these ladder operators. In principle, the basis $\{|n\rangle\}_{n=0,1,2,\dots}$ is infinite, but for practical purposes we truncate it after a large, but finite number of states: $|0\rangle, |1\rangle, \dots, |N\rangle$. However, as the harmonic oscillator states do not constitute an eigenbasis of the Hamiltonian, this representation is not diagonal and the energy eigenvalues have to be determined numerically [32]. For all calculations, we have retained $N = 500$ harmonic oscillator states for finding Landau levels. In our trials, it was observed that retaining fewer Landau levels resulted in large deviations in energy eigenvalues at low magnetic fields, while retaining more than 500 Landau levels resulted in very large execution times without any significant improvement in accuracy.

Landau level spectra obtained in this way have been plotted in Fig. 2. The most striking feature of these plots is the dispersion of energies with respect to magnetic field, for example, in monolayer Landau levels go as $E_n \sim \sqrt{B}$, while for AB bilayer dispersion is linear, $E_n \sim B$. In TBG, especially at magic angles, the peculiar nature of flat bands near zero energy should be noted. On the other hand, dispersion of higher Landau levels with respect to magnetic field gets very steep when twist is in magic range. At larger twist angles, as the two layers get decoupled, qualitative features of the TBG spectrum and the dispersion with respect to magnetic field are very similar to monolayer, except for a renormalized Fermi velocity [16, 25]. In fact, efficiency of Otto cycle depends, almost exclusively,

on dispersion of Landau levels with respect to magnetic field. This is discussed in detail in Section IV.

III. QUANTUM HEAT ENGINE CYCLE

For the heat engine, we consider an ensemble of single electron states in the conduction band [12–14]. We take Landau levels $|\psi_n\rangle$ with energies E_n and occupation probabilities p_n , so that the density matrix $\rho = \sum_n p_n |\psi_n(B)\rangle \langle \psi_n(B)|$. Average energy of this ensemble, $U = \text{Tr}(\rho \mathcal{H}_\theta) = \sum_n p_n E_n$ is identified as *internal energy* of the system, and we can state a quantum version of the first law of thermodynamics [1, 3, 10],

$$dU = dQ + dW = \sum_n E_n dp_n + \sum_n p_n dE_n. \quad (12)$$

Since thermodynamic entropy $S = -k_B \sum_n p_n \ln p_n$, and in classical thermodynamics, heat exchanged $dQ = TdS$, we identify $dQ = \sum_n E_n dp_n$ and work as $dW = \sum_n p_n dE_n$ [1, 3, 10]. From density matrix, we can calculate von Neumann entropy,

$$S(T, B) = -k_B \text{Tr}(\rho \ln \rho) = -k_B \sum_n p_n \ln p_n. \quad (13)$$

Occupation probabilities of different energy levels are determined by temperature of working substance [1, 12]. Temperature of working substance is controlled either by keeping it in equilibrium with a heat bath and varying its temperature quasistatically, or by coupling it to hot and cold reservoirs alternatively [4, 6, 22]. At temperature T , occupation probabilities satisfy Boltzmann distribution which is given as,

$$p_n(T, B) = \frac{e^{-\beta E_n(B)}}{Z(T, B)}; \quad Z(T, B) = \sum_{n=0}^{\infty} e^{-\beta E_n(B)}, \quad (14)$$

with $\beta = 1/k_B T$ and $Z(T, B)$ being partition function. In what follows, we shall assume that the thermal reservoir is a classical object and that its temperature can be varied quasistatically. We shall also assume that external magnetic field can be varied quasistatically to modulate Landau levels E_n , and their occupation probabilities p_n .

Quantum Otto cycle consists of four strokes, operating between magnetic field strengths B_1 and B_2 (with $B_2 > B_1$), and temperatures T_C and T_H (with $T_H > T_C$). Temperature of reservoir is controlled such that it goes from T_C to T_H via T_2 and back to T_C via T_4 (see Fig. 3). In order to draw parallels with classical Otto cycle, it is easier to state the compression and expansion strokes in terms of decreasing and increasing Landau radius.

The first stroke is an adiabatic compression in which Landau radius is reduced by gradually increasing the external magnetic field. Due to this changing magnetic field, we have $l_{B_1} \rightarrow l_{B_2}$. However, since entropy is held constant, temperature must also change $T_C \rightarrow T_2$, to satisfy adiabatic condition $\Delta S = 0$. If all energy levels change in the same ratio, the working substance remains in a thermal state with a well defined temperature at the end of an adiabatic process [1]. This is exactly what happens

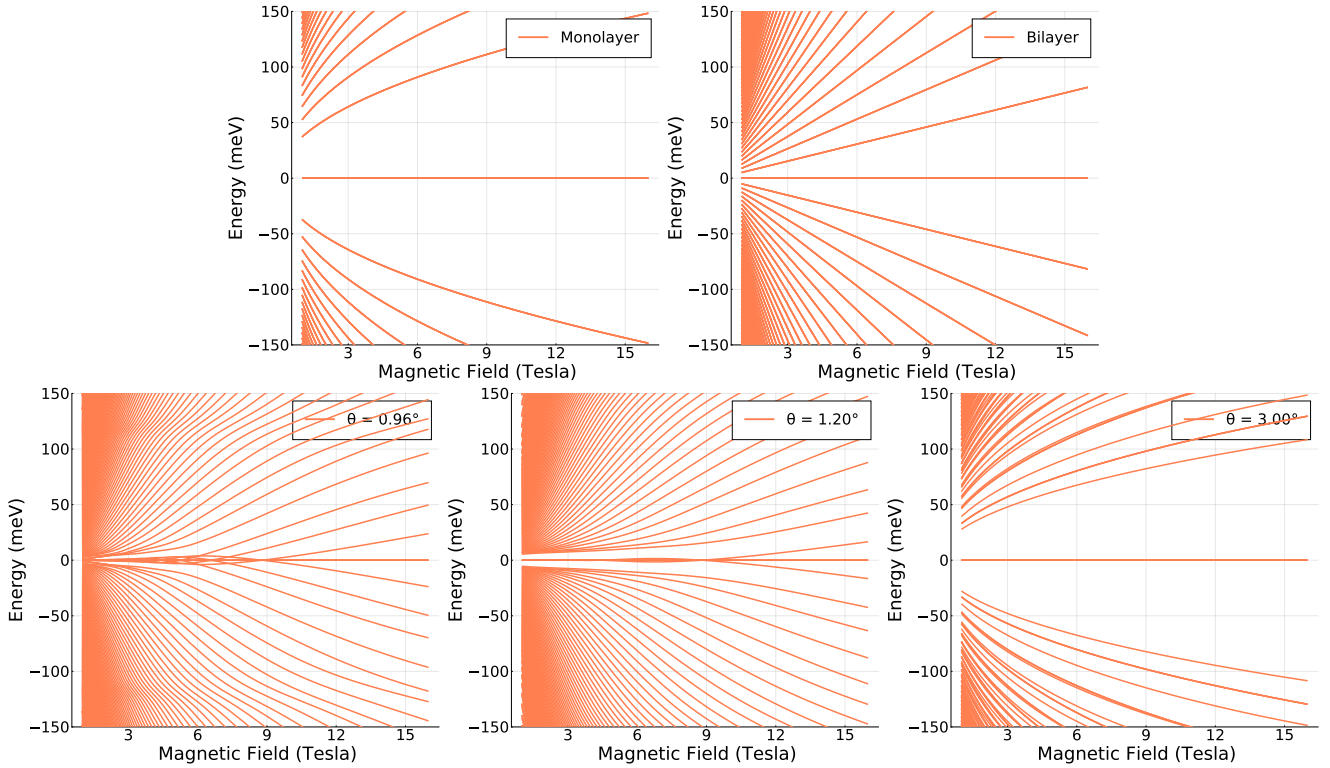


FIG. 2. Landau level spectra for monolayer, AB stacked bilayer and twisted bilayer graphene. The most important feature of these plots is the dispersion of energy levels with respect to the magnetic field. For monolayer Landau levels go as $E_n \sim \sqrt{B}$, for bilayer the dispersion is linear $E_n \sim B$. With a small twist, Landau levels around zero energy start having a flat dispersion, and as twist is increased the Landau level spectrum starts looking remarkably similar to the monolayer. Peculiar nature of magic angle induced flat bands near zero energy for $\theta^* = 0.96^\circ$ should be noted.

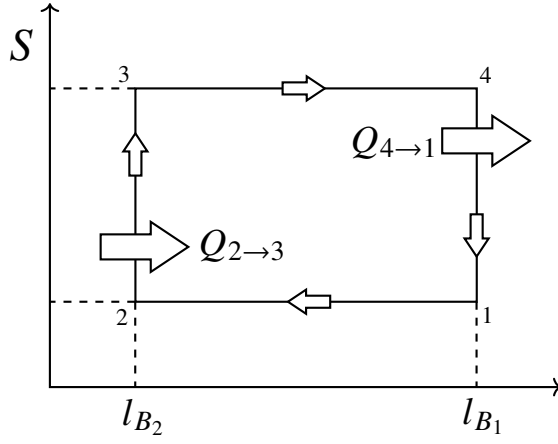


FIG. 3. Four strokes of Otto cycle on an entropy–magnetic field plot. The cycle starts with an adiabatic compression $1 \rightarrow 2$, in which Landau radius decreases due to an increase in magnetic field, followed by an isochoric absorption of heat $2 \rightarrow 3$. Next, magnetic field is decreased adiabatically $3 \rightarrow 4$ and finally heat is rejected isochorically $4 \rightarrow 1$ to return the system to its initial state.

for Landau levels in graphene under a changing magnetic field. Hence, we can safely assume that the system is at a well-defined temperature T_2 at the end of this first stroke. Similar arguments

apply for adiabatic expansion stroke $3 \rightarrow 4$.

If magnetic field is changed very slowly, we can use quantum adiabatic theorem to conclude $dP_n = 0$, and therefore $dQ_{1 \rightarrow 2} = \sum_n E_n dP_n = 0$ and the process is thermodynamically adiabatic. The intermediate temperature T_2 is determined by the condition

$$S(T_C, B_1) = S(T_2, B_2). \quad (15)$$

In second stroke, temperature of working substance is increased from T_2 to T_H as it absorbs heat from reservoir, while Landau radius is held constant at l_{B_2} . This process is called a *hot isochore* [6, 22]. Heat absorbed in this stroke can be calculated from (12),

$$Q_{2 \rightarrow 3} = \int_2^3 \sum_{n=0}^{\infty} E_n(B_2) dP_n = \sum_{n=0}^{\infty} E_n(B_2) [p_n(T_H, B_2) - p_n(T_2, B_2)] \quad (16)$$

The next stroke is an adiabatic expansion and involves an increase of Landau radius $l_{B_2} \rightarrow l_{B_1}$, while lowering of temperature $T_H \rightarrow T_4$ such that the adiabatic condition

$$S(T_H, B_2) = S(T_4, B_1), \quad (17)$$

is satisfied. This stroke, like $1 \rightarrow 2$, is carried out very slowly so that quantum adiabatic theorem can be applied and $dQ_{3 \rightarrow 4} = 0$. T_4 can be determined from adiabatic condition (17).

In the final stroke, temperature decreases from T_4 to T_C , as heat is lost to reservoir, with Landau radius being held constant at l_{B_1} . This process is called a *cold isochore* [6, 22]. Heat exchanged in this stroke can be calculated as before,

$$Q_{4 \rightarrow 1} = \sum_{n=0}^{\infty} E_n(B_1) [p_n(T_C, B_1) - p_n(T_4, B_1)]. \quad (18)$$

Since no heat exchange occurs in adiabatic processes, and working substance returns to its initial state at end of cycle, we can use quantum first law with $\Delta U = 0$ to write work output of engine as

$$|W_O| = Q_{\text{cycle}} = |Q_{2 \rightarrow 3}| - |Q_{4 \rightarrow 1}|, \quad (19)$$

while efficiency is given by,

$$\eta_O = \left| \frac{W_O}{Q_{\text{in}}} \right| = \frac{|Q_{2 \rightarrow 3}| - |Q_{4 \rightarrow 1}|}{|Q_{2 \rightarrow 3}|} = 1 - \left| \frac{Q_{4 \rightarrow 1}}{Q_{2 \rightarrow 3}} \right| \quad (20)$$

$$= 1 - \left| \frac{\sum_n E_n(B_1) [p_n(T_C, B_1) - p_n(T_4, B_1)]}{\sum_n E_n(B_2) [p_n(T_H, B_2) - p_n(T_2, B_2)]} \right|, \quad (21)$$

where in the last line, we used (16) and (18). Discussion up to this point has been completely general, since all these results are direct consequences of the quantum first law of thermodynamics. Eqs. (19) and (21) are equally applicable to any quantum working substance coupled to a classical thermal reservoir. Very similar expressions for work and efficiency appear, for example, in [1, 3, 12–14].

IV. RESULTS AND DISCUSSION

A. Efficiency

In case of *AB* stacked bilayer graphene, where an analytical expression for Landau levels is known, we can use (21) and the quantum adiabatic conditions—

$$p_n(T_C, B_1) = p_n(T_2, B_2), \quad p_n(T_H, B_2) = p_n(T_4, B_1) \quad (22)$$

to derive the Otto efficiency,

$$\eta_O^{\text{bi}} = 1 - \left| \frac{\omega_{B_1}}{\omega_{B_2}} \right| = 1 - \left(\frac{l_{B_2}}{l_{B_1}} \right)^2 = 1 - r_C^{-2}, \quad (23)$$

where we have defined the *compression ratio* $r_C = l_{B_1}/l_{B_2}$ so that the efficiency is reminiscent of the classical expression $\eta_O = 1 - r_C^{-(\gamma-1)}$ [33]. Similarly, for monolayer graphene, we have

$$\eta_O^m = 1 - \left| \frac{l_{B_2}}{l_{B_1}} \right| = 1 - r_C^{-1}. \quad (24)$$

In fact, if Landau level energies have a simple dispersion with respect to Landau radius, $E_n(B) = l_B^{-\alpha} f(n)$, then it immediately follows from (21) and (22) that efficiency of the quantum Otto cycle is,

$$\eta_O = 1 - r_C^{-\alpha}. \quad (25)$$

For magic angle twisted bilayer graphene, a simple expression for Landau level energies is not known, and therefore an analytic expression for efficiency cannot be derived. Hence, temperatures T_2 and T_4 have to be determined numerically from adiabatic conditions (15) and (17), and efficiency has to be computed directly from (21). For all numerical computations in this work $B_1 = 5$ T, $T_C = 30$ K and $T_H = 100$ K were fixed, and $N = 500$ Landau levels were retained (see [32]).

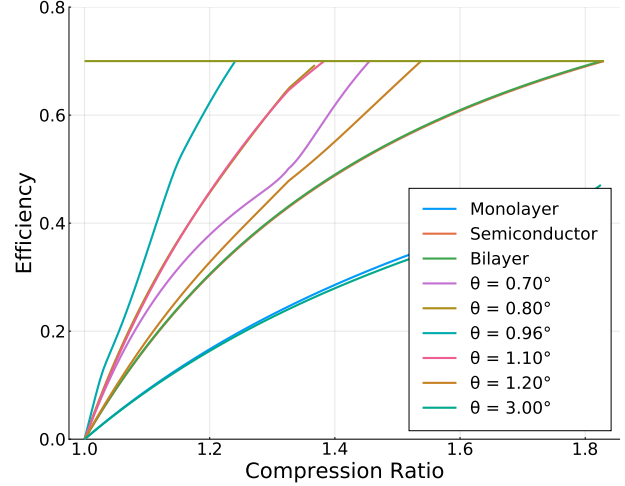


FIG. 4. Efficiencies as a function of the compression ratio for cycles operating between $T_C = 30$ K and $T_H = 100$ K, and $B_1 = 5.0$ T. Different twist angles are plotted together for comparison.

Efficiencies as a function of the compression ratio, obtained by direct numerical computation, can be fitted for the parameter α in (25). In fact, some partial insight into increased efficiencies can be ascertained by looking at qualitative differences in Landau level plots for monolayer, bilayer, and magic angle twisted bilayer graphene. If the Landau levels are $E_n(B) = l_B^{-\alpha} f(n) = (eB/\hbar)^{\alpha/2} f(n)$, then efficiency is given by $\eta_O = 1 - r_C^{-\alpha}$. Hence, a larger value of α in dispersion of E_n is responsible for higher efficiency, and this is exactly what we see in Landau level plots for twisted bilayer. After attaining a maximum at $\theta^* = 0.96^\circ$ (magic angle) the efficiency starts falling for larger twist angles until it coincides with monolayer efficiency for $\theta = 3.0^\circ$. This is to be expected, because for larger twist angles because the two layers get decoupled. The take-home message of our paper is the following: proposed quantum Otto engine has the highest efficiency at magic angle $\theta^* = 0.96^\circ$.

In Fig. 4, we notice identical efficiencies for the semiconductor quantum dot and *AB* stacked bilayer graphene. This is because, in a semiconductor quantum dot under a cylindrical potential well of the form

$$V_{\text{dot}} = \frac{m_{\text{eff}}}{2} \omega_d^2 (x^2 + y^2), \quad (26)$$

Landau levels are given by

$$E_{n,m} = \hbar\Omega(2n + |m| + 1) - m \frac{\hbar\omega_B}{2}, \quad (27)$$

where $\Omega = [\omega_d^2 + \omega_B^2/4]^{1/2}$ [12]. Therefore, the spectrum disperses as $E_{n,m} \sim l_B^{-2}$ except for a correction due to the geometric confinement ω_d . In light of discussions in the preceding paragraph, it is not surprising why efficiencies coincide.

B. Work

Work output is obtained by directly computing the difference between heat absorbed (16) and heat lost (18) during the cycle. Work is plotted as function of compression ratio in Fig. 5. For each case, work output initially increases as compression ratio is increased, and after attaining a maximum starts falling and eventually reaches zero just as efficiency reaches Carnot limit $\eta_C = 1 - T_C/T_H = 0.7$. Zero work output at Carnot efficiency can be interpreted as a manifestation of the second law of thermodynamics in these systems. In particular, we note that the proposed heat engine cannot surpass the Carnot limit despite operating with a quantum working substance as the cycle is composed of equilibrium processes, committed to operate between two temperatures [4, 12, 34].

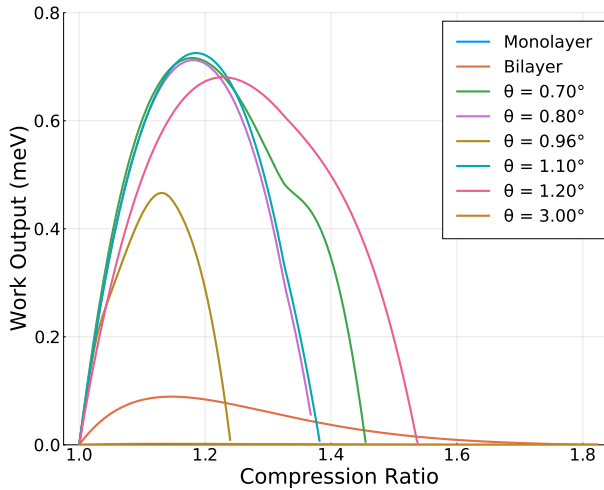


FIG. 5. Work output as a function of compression ratio at different twist angles, for cycles operating between $T_C = 30$ K and $T_H = 100$ K, and magnitude $B_1 = 5.0$ T. Different twist angles are plotted together for comparison.

Finally, we note that work outputs in Fig. 5 do not show any strong correlations with twist angle, except for a dip at the magic angle. Due to flat bands at magic angle, Landau levels which are predominantly occupied during the cycle (see Eq. 14), have energy very close to zero. Hence (16) and (18) imply that the heat absorbed and rejected during the cycle are significantly smaller, which results in a lower work output.

V. CONCLUSION

In this work we explored the possibility of exploiting magic angles of twisted bilayer graphene to design a highly efficient magnetic quantum heat engine. We have shown that a quantum

TABLE I. A comparison of efficiencies and work outputs

Working Substance	Efficiency	Work (meV)
Monolayer Graphene	$1 - r_C^{-1.00}$	0.000169
Semiconductor	$1 - r_C^{-1.98}$	1.143
Bilayer Graphene	$1 - r_C^{-2.00}$	0.0758
	$\theta = 0.70^\circ$	$1 - r_C^{-2.68}$
	$\theta = 0.80^\circ$	$1 - r_C^{-3.48}$
Twisted Bilayer	$\theta^* = 0.96^\circ$	$1 - r_C^{-5.03}$
	$\theta = 1.10^\circ$	$1 - r_C^{-3.47}$
	$\theta = 1.20^\circ$	$1 - r_C^{-2.37}$
	$\theta = 3.00^\circ$	$1 - r_C^{-0.98}$
		0.00159

Otto engine based on magic angle twisted bilayer graphene exhibits a much greater efficiency than one based on either monolayer or bilayer graphene, or a semiconductor quantum dot. Efficiency varies smoothly with twist and achieves a maximum at the magic angle. On the other hand, it falls as the two layers get decoupled for larger twists, and for $\theta = 3.0^\circ$ coincides with that of monolayer. These results were also related with the qualitative features of Landau fan plots for monolayer, bilayer and twisted bilayer graphene.

Analytical expressions for efficiency with the generic form $\eta_0 = 1 - r_C^{-\alpha}$ were derived for monolayer and *AB* stacked bilayer graphene with $\alpha = 1$ and $\alpha = 2$ respectively. Efficiencies were computed numerically for magic angle twisted bilayer and parameter α was fitted with the results. It was observed that the Otto cycle is extremely efficient at magic angle twist $\theta^* = 0.96^\circ$ with $\alpha = 5.03$. Results for different twist angles have been presented in Table I for comparison.

We end by noting that a Carnot cycle with MATBG can be designed analogously, by using two adiabatic and two isothermal strokes. While the efficiency of a Carnot cycle is fixed at $\eta_C = 1 - T_C/T_H$ independent of expansion ratio [1, 12], it will be interesting to see what impact magic angle twists have on work output. After looking at a highly efficient quantum heat engine based on MATBG, a natural question to ask next is if it might be possible to use MATBG to design a nanoscale refrigerator with a high coefficient of performance. Both these possibilities will be explored in a future work [35].

[1] H. T. Quan, Y.-x. Liu, C. P. Sun, and F. Nori, Quantum thermodynamic cycles and quantum heat engines, *Phys. Rev. E* **76**, 031105 (2007).

[2] H. T. Quan, Quantum thermodynamic cycles and quantum heat engines. ii., *Phys. Rev. E* **79**, 041129 (2009).

[3] H. T. Quan, P. Zhang, and C. P. Sun, Quantum heat engine with

multilevel quantum systems, *Phys. Rev. E* **72**, 056110 (2005).

[4] S. Vinjanampathy and J. Anders, Quantum thermodynamics, *Contemporary Physics* **57**, 545 (2016).

[5] M. O. Scully, Extracting work from a single thermal bath via quantum negentropy, *Phys. Rev. Lett.* **87**, 220601 (2001).

[6] J. Roßnagel, O. Abah, F. Schmidt-Kaler, K. Singer, and E. Lutz, Nanoscale heat engine beyond the carnot limit, *Phys. Rev. Lett.* **112**, 030602 (2014).

[7] M. O. Scully, K. R. Chapin, K. E. Dorfman, M. B. Kim, and A. Svidzinsky, Quantum heat engine power can be increased by noise-induced coherence, *Proceedings of the National Academy of Sciences* **108**, 15097 (2011), <https://www.pnas.org/content/108/37/15097.full.pdf>.

[8] M. O. Scully, M. S. Zubairy, G. S. Agarwal, and H. Walther, Extracting work from a single heat bath via vanishing quantum coherence, *Science* **299**, 862 (2003), <https://science.sciencemag.org/content/299/5608/862.full.pdf>.

[9] K. E. Dorfman, D. V. Voronine, S. Mukamel, and M. O. Scully, Photosynthetic reaction center as a quantum heat engine, *Proceedings of the National Academy of Sciences* **110**, 2746 (2013), <https://www.pnas.org/content/110/8/2746.full.pdf>.

[10] T. D. Kieu, The second law, maxwell's demon, and work derivable from quantum heat engines, *Phys. Rev. Lett.* **93**, 140403 (2004).

[11] S. Toyabe, T. Sagawa, M. Ueda, E. Muneyuki, and M. Sano, Experimental demonstration of information-to-energy conversion and validation of the generalized jarzynski equality, *Nature Physics* **6**, 988 (2010).

[12] E. Muñoz and F. J. Peña, Magnetically driven quantum heat engine, *Phys. Rev. E* **89**, 052107 (2014).

[13] F. J. Peña, O. Negrete, G. Alvarado Barrios, D. Zambrano, A. González, A. S. Nunez, P. A. Orellana, and P. Vargas, Magnetic otto engine for an electron in a quantum dot: Classical and quantum approach, *Entropy* **21**, 10.3390/e21050512 (2019).

[14] F. J. Peña and E. Muñoz, Magnetostrain-driven quantum engine on a graphene flake, *Phys. Rev. E* **91**, 052152 (2015).

[15] F. J. Peña, D. Zambrano, O. Negrete, G. De Chiara, P. A. Orellana, and P. Vargas, Quasistatic and quantum-adiabatic otto engine for a two-dimensional material: The case of a graphene quantum dot, *Phys. Rev. E* **101**, 012116 (2020).

[16] R. Bistritzer and A. H. MacDonald, Moiré bands in twisted double-layer graphene, *Proceedings of the National Academy of Sciences* **108**, 12233 (2011), <https://www.pnas.org/content/108/30/12233.full.pdf>.

[17] J. M. B. Lopes dos Santos, N. M. R. Peres, and A. H. Castro Neto, Continuum model of the twisted graphene bilayer, *Phys. Rev. B* **86**, 155449 (2012).

[18] Y. Cao, V. Fatemi, S. Fang, K. Watanabe, T. Taniguchi, E. Kaxiras, and P. Jarillo-Herrero, Unconventional superconductivity in magic-angle graphene superlattices, *Nature* **556**, 43 (2018).

[19] Y. Cao, V. Fatemi, A. Demir, S. Fang, S. L. Tomarken, J. Y. Luo, J. D. Sanchez-Yamagishi, K. Watanabe, E. Kaxiras, R. C. Ashoori, and P. Jarillo-Herrero, Correlated insulator behaviour at half-filling in magic-angle graphene superlattices, *Nature* **556**, 80 (2018).

[20] K. Hejazi, C. Liu, and L. Balents, Landau levels in twisted bilayer graphene and semiclassical orbits, *Phys. Rev. B* **100**, 035115 (2019).

[21] Y.-H. Zhang, H. C. Po, and T. Senthil, Landau level degeneracy in twisted bilayer graphene: Role of symmetry breaking, *Phys. Rev. B* **100**, 125104 (2019).

[22] O. Abah, J. Roßnagel, G. Jacob, S. Deffner, F. Schmidt-Kaler, K. Singer, and E. Lutz, Single-ion heat engine at maximum power, *Phys. Rev. Lett.* **109**, 203006 (2012).

[23] J. M. B. Lopes dos Santos, N. M. R. Peres, and A. H. Castro Neto, Graphene bilayer with a twist: Electronic structure, *Phys. Rev. Lett.* **99**, 256802 (2007).

[24] R. Bistritzer and A. H. MacDonald, Moiré butterflies in twisted bilayer graphene, *Phys. Rev. B* **84**, 035440 (2011).

[25] J. Python, *Quantum oscillations in twisted bilayer graphene*, Master's thesis, Utrecht University (2019).

[26] M. O. Goerbig, Electronic properties of graphene in a strong magnetic field, *Rev. Mod. Phys.* **83**, 1193 (2011).

[27] E. McCann and M. Koshino, The electronic properties of bilayer graphene, *Reports on Progress in Physics* **76**, 056503 (2013).

[28] A. H. Castro Neto, F. Guinea, N. M. R. Peres, K. S. Novoselov, and A. K. Geim, The electronic properties of graphene, *Rev. Mod. Phys.* **81**, 109 (2009).

[29] E. McCann and V. I. Fal'ko, Landau-level degeneracy and quantum hall effect in a graphite bilayer, *Phys. Rev. Lett.* **96**, 086805 (2006).

[30] R. de Gail, M. O. Goerbig, F. Guinea, G. Montambaux, and A. H. Castro Neto, Topologically protected zero modes in twisted bilayer graphene, *Phys. Rev. B* **84**, 045436 (2011).

[31] P. Moon and M. Koshino, Energy spectrum and quantum hall effect in twisted bilayer graphene, *Phys. Rev. B* **85**, 195458 (2012).

[32] Julia code used to determine (a) Landau levels numerically for MATBG is available at <https://github.com/11DE784A/bilayer/blob/9640d61330b81cb22ab0fe65bdcba6d73da27475/Spectra.jl> (b) efficiencies and work done for quantum Otto engine with TBG is available at <https://github.com/11DE784A/bilayer/blob/9640d61330b81cb22ab0fe65bdcba6d73da27475/Otto.jl>.

[33] $\gamma = C_p/C_V$ is the ratio of specific heats at constant pressure and constant volume.

[34] W. Niedenzu, D. Gelbwaser-Klimovsky, and G. Kurizki, Performance limits of multilevel and multipartite quantum heat machines, *Phys. Rev. E* **92**, 042123 (2015).

[35] A. Singh and C. Benjamin, Manuscript under preparation.